

Thermal Decomposition Enhancement of HMX by Bonding with TiO₂ Nanoparticles

Qing Zhu,*^[a] Chun Xiao,^[a] Xiao Xie,^[a] Bao-hui Zheng,^[a] Shang-bin Li,^[a] and Guan Luo^[a]

Abstract: The appropriate structure and properties of a composite material, including the morphology, particle size, and bond strength, are very important for its performance and practical applications. The energetic material HMX ($C_4H_8N_8O_8$, cyclotetramethylenetrinitramine) is typically mixed with nanocatalysts to improve its thermal decomposition, which is advantageous for its detonation performance in practical applications. Inspired by the bioadhesion of mussels, a HMX@PDA@TiO₂ (HMX first coated with PDA film and second coated with TiO₂ nanoparticles) composite was developed in this study to greatly advance the thermal decomposition temperatures. A simple stirring process was used to prepare the composite from HMX and TiO₂ nano-

particles under dopamine solutions with different pH values. Nanocatalyst TiO₂ nanoparticles were anchored on the surface of HMX by reacting with the dopamine and poly-dopamine coatings. Compared with other reference samples, the thermal behavior of the obtained composite showed that the starting decomposition temperature was lower, at approximately 60 °C, and that the decomposition peak decreased by 35 °C, indicating that the composite properties should have great effects on the thermal performance of the materials. The findings offer a valuable composite preparation method to enhance the thermal behavior and the effect of the catalyst on the composite via bonding effects.

Keywords: TiO₂ nanoparticles · HMX · Nanocatalyst · Thermal decomposition · Bonding effects

1 Introduction

When a composite is prepared with different materials, the composite is typically used to improve the properties of the component, such as the mechanical performance [1, 2], catalytic performance [3, 4], thermal decomposition [5, 6], and surface wettability [7, 8]. However, the structure and properties of composites, including the morphologies [9], particle sizes [10], and bond strengths [11], are very important for their performances [12]. An appropriate preparation method for a composite to provide better composite properties is advantageous for their performance and practical applications [13].

HMX ($C_4H_8N_8O_8$, cyclotetramethylenetrinitramine) is one of the most common energetic materials used in propellants, explosives and pyrotechnics [14, 15], owing to its high detonation heat, detonation velocity and detonation pressure [16, 17]. The combustion performance of HMX, which is one of a most focused property in propellants, is affected by its thermal behavior [16], and some catalytic agents have been mixed with HMX to regulate its thermal properties [18]. Because of their high specific surface areas and surface activations, nanocatalysts with sizes of 1~100 nm, including metallic and metal oxide nanoparticles, are the most widely studied and used catalytic agents in energetic material applications [19~21]. However, metallic nanoparticles, such as commonly used Al nanoparticles [22, 23], are not stable in air and increase the difficulty of operation [24]. Therefore, metal oxide nanoparticles are like-

ly better catalytic agents in practical applications as for more stable and lower cost under the room ambient.

Traditionally, nanocatalysts are only added into energetic materials to prepare the mixture for the thermal behavior measurements. Although certain improvements are observed, and there are still some drawbacks to the mixing process. The weight content of nanocatalyst is always between 1%~10%, which will influence other characteristics of the mixture. More importantly, nanocatalysts do not exhibit uniform bonding characteristics with the energetic materials, and the space between the nanocatalysts and the energetic materials in the mixture will reduce the contact area and number of activation points, which will decrease the catalytic properties and influence the thermal behavior. To improve these properties, a composite with bonding characteristics could be a better option to further enhance the combustion performance of the energetic materials.

In this study, inspired by the bioadhesion of mussels [25, 26], we report nanocatalyst TiO₂ nanoparticles anchored via bonding on the surface of HMX. A simple stirring process was developed to prepare the HMX@PDA@TiO₂ composite from HMX and TiO₂ nanoparticles in dopamine solutions with different pH values. TiO₂ nanoparticles were

[a] Q. Zhu, C. Xiao, X. Xie, B.-h. Zheng, S.-b. Li, G. Luo

Institute of Chemical Materials
China Academy of Engineering Physics
Mianyang, Sichuan 621999, P.R.China
*e-mail: zhuqing@caep.cn

homogeneously and closely deposited on the surface of HMX, and the TiO_2 mass ratio in the composite was considered negligible. Compared with the reference samples, the thermal behavior of the obtained composite showed that the starting decomposition temperature was lower, at approximately 60°C , and the decomposition peak reduced to 35°C , indicating that the composite properties should greatly affect their thermal performance. The findings in this study offer a simple method for preparing a composite between energetic materials and nanocatalysts to enhance the thermal decomposition performance, which could be valuable for catalytic and energetic material fields.

2 Experimental Section

2.1 Materials

HMX with an average size of approximately $450\ \mu\text{m}$ was used as the starting particles. Dopamine hydrochloride (DA), 2-amino-2-hydroxymethylpropane-1,3-diol (Tris) and amino-propyl trimethoxysiloxane were supplied by Aladdin Chemical, Ltd. (Shanghai, China). Acetic acid and sodium dodecyl sulfate were purchased from Kelong Chemical Corporation in Chengdu. The TiO_2 nanoparticles used in the experiments were provided by Degussai with an average size of approximately 25 nm. All reagents were used as-received without any purification.

2.2 Reference Samples in the Decomposition Experiments

The original HMX particles were washed with deionized water and ethanol several times and dried in 50°C before use.

HMX@PDA: 2 g of HMX was added in 250 mL of a dopamine-Tris solution ($2\ \text{mg mL}^{-1}$, $\text{pH}=8.5$, 10 mM Tris-HCl buffer) under stirring for 12 h at room temperature. Then, the particles were separated from dispersion and washed with deionized water several times, followed by dried in 50°C to obtain HMX@PDA particles.

HMX- TiO_2 : 2 g of HMX was immersed in 50 mL of amino-propyl trimethoxysiloxane-ethanol solution (5 mM) for 30 min at room temperature. The filtered HMX was dispersed in 20 mL water with the addition of 3 mL acetic acid, and 0.4 g TiO_2 nanoparticles were also ultrasonically dispersed in 20 mL water with the addition of 40 mg of sodium dodecyl sulfate. Then, the two kinds of dispersions were mixed and stirred for 1 min and the resultant HMX- TiO_2 was washed with deionized water and dried in 70°C before measurement.

2.3 Preparation of the HMX@PDA@ TiO_2 Composite

Typically, TiO_2 nanoparticles with different concentrations ($0\ \text{mg mL}^{-1}$, $5\ \text{mg mL}^{-1}$, $10\ \text{mg mL}^{-1}$, $20\ \text{mg mL}^{-1}$, $30\ \text{mg mL}^{-1}$ and $40\ \text{mg mL}^{-1}$) and 4 mg mL^{-1} dopamine hydrochloride were dispersed in 30 mL solution at pH 3 by ultrasonication for 20 min. The pH values of the solutions were adjusted by acetic acid. Then, 2 g of HMX@PDA particles was added in the mixture under stirring for 6 h. After washing with water several times and drying at 50°C , the resultant HMX@PDA@ TiO_2 composite was obtained for thermal analysis.

2.4 Characterizations

The morphologies of the samples were observed by scanning electron microscopy (SEM, CamScan Apollo300). Brunauer-Emmett-Teller (BET) surface area measurements were characterized on a Quantachrome NOVA2000. Fourier transform infrared spectra (FT-IR) were obtained by a BRUKER VERTEX70 with a range of $400\ \text{cm}^{-1}\sim4000\ \text{cm}^{-1}$. X-ray diffraction (XRD) measurements were carried out on a Shimadzu XRD-6000. X-ray photoelectron spectroscopy (XPS) was performed on a PHI-5700ESCA. TG-DSC measurements were recorded by a NETZSCH STA 449 C at a heating rate of $2\ ^\circ\text{C min}^{-1}$, $5\ ^\circ\text{C min}^{-1}$, $10\ ^\circ\text{C min}^{-1}$, and $20\ ^\circ\text{C min}^{-1}$ under nitrogen atmosphere. Combustion was investigated using 50 mg sample at room ambient and the processes were observed with a high speed video (5000 fps).

3 Results and Discussions

3.1 Morphology of the as-Prepared HMX@PDA@ TiO_2 Composite

The surfaces of the original HMX and HMX@PDA particles were smooth and uniform, as shown in our previous work [14]. The surface morphology of the HMX@PDA@ TiO_2 composites was observed by SEM, as shown in Figure 1. TiO_2 nanoparticles anchored on the surfaces of HMX to form the micro-nanostructures, and the TiO_2 aggregation became more obvious with the increasing concentration of TiO_2 in the dispersions. The TiO_2 nanoparticles formed a thin film on the HMX surface at the concentration of $5\ \text{mg mL}^{-1}$, and then, the TiO_2 nanoparticles completely covered and formed many raised nanoscale structures on the HMX surface at the concentration of $10\ \text{mg mL}^{-1}$. Because of the more abundant contacting opportunities between the TiO_2 nanoparticles and HMX with higher TiO_2 dispersion concentrations, the differences of the surface structures and the amount of coverage of TiO_2 could be determined for the resultant HMX@PDA@ TiO_2 composites.

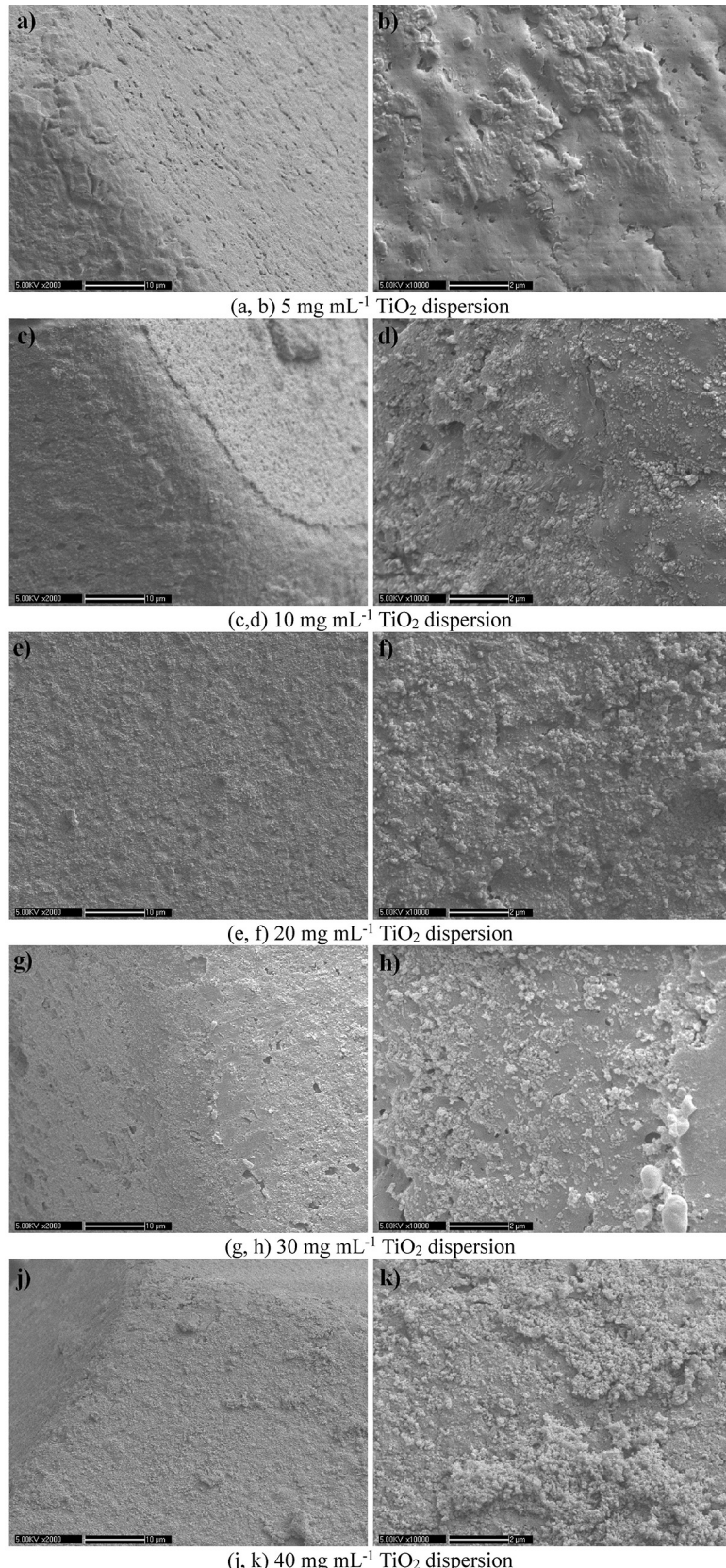


Figure 1. SEM images of the HMX@PDA@ TiO_2 composites with different TiO_2 dispersion concentrations under $\times 2000$ (left) and $\times 10000$ (right) magnification.

3.2 Structures of the HMX@PDA@ TiO_2 Composite

The resultant HMX@PDA@ TiO_2 composite prepared under the 10 mg mL^{-1} TiO_2 dispersion was used for the structural characterization. The BET surface area of the composite was $0.96 \text{ m}^2 \text{ g}^{-1}$, which is larger than the original HMX and HMX@PDA (the measurement data were shown in our previous work), owing to the nanostructures formed by the TiO_2 nanoparticles on the surfaces. The XRD pattern of the composite confirmed that the 2θ values of 14.70° , 16.06° , 20.50° , 23.06° , 26.16° , 27.26° , 29.71° , 31.97° , 37.12° and 41.27° were consistent with β -HMX [27], and the 2θ values of 25.33° , 37.82° , 48.05° , 50.83° , 53.88° and 55.06° were the characteristic peaks of anatase TiO_2 [28] in the region of $10\text{--}60^\circ$ in Figure 2, which demonstrated that the TiO_2 nanoparticles were deposited on the HMX surface.

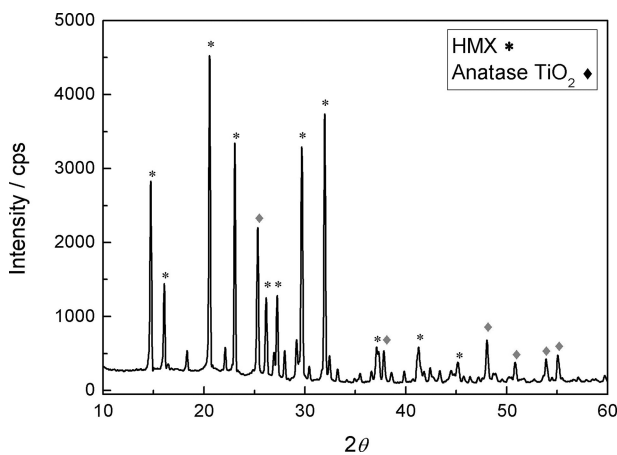


Figure 2. XRD pattern of the HMX@PDA@ TiO_2 composite.

The comparison of the FTIR spectra for the TiO_2 nanoparticles, HMX@PDA and the HMX@PDA@ TiO_2 composite are shown in Figure 3. For both the original TiO_2 and HMX@PDA, the broad O–H stretching absorption peak at 3150 cm^{-1} associated with the OH groups on the surfaces of TiO_2 and polydopamine [29]. However, the broad hydroxyl peaks changed to two weak peaks at 3035 cm^{-1} and 3074 cm^{-1} in the composite, and some new absorption peaks at 785 cm^{-1} , 1039.4 cm^{-1} , 1432.8 cm^{-1} and 1593 cm^{-1} emerged, which were attributed to the aryl–oxygen stretch vibration and $\text{O}-\text{Ti}-\text{O}$ groups formed by dopamine and the TiO_2 reaction [29, 30]. Figure 4 and Table 1 show the XPS spectra and the elemental content of the composite. The survey spectrum displayed that the surface elements not only contained C, N, and O but also contained Ti, which can be confirmed from the elemental content table. The Ti 2p spectrum could be divided into four components at 458.8 eV , 460.1 eV , 464.2 eV , and 465.87 eV , corresponding to $\text{O}-\text{Ti}-\text{O}$, $\text{Ti } 2p_{3/2}$ and $\text{Ti } 2p_{1/2}$ in TiO_2 [31], respectively, which is also supported by the peak at 530.9 eV in the O 1s spec-

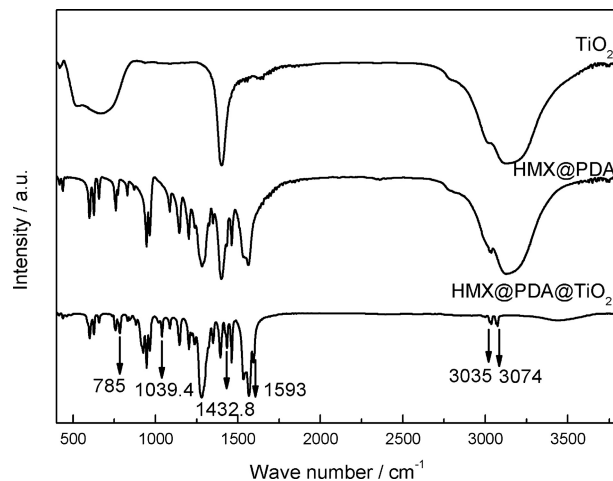


Figure 3. FTIR spectra of TiO_2 , HMX@PDA and HMX@PDA@ TiO_2 .

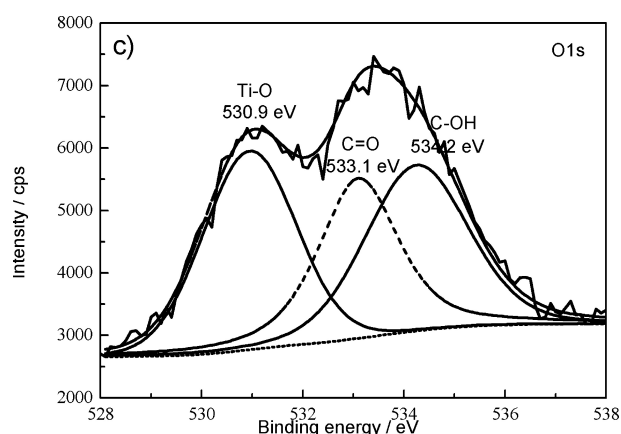


Figure 4. XPS spectra of the HMX@PDA@ TiO_2 composite.

Table 1. Elemental content of the HMX@PDA@ TiO_2 composite.

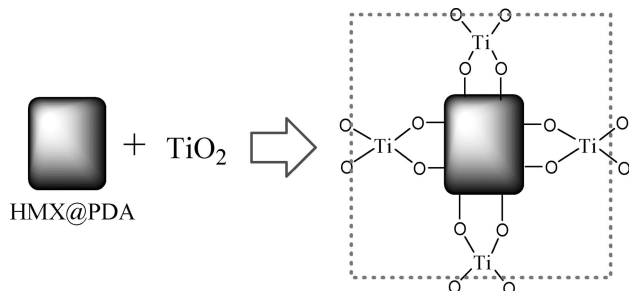
Samples	Elemental content (%)			
	C	O	N	Ti
HMX@PDA	40.98	29.16	29.86	0
HMX@PDA@ TiO_2	43.71	31.95	17.84	6.5

trum, corresponding to Ti–O [32]. The species suggest that the TiO_2 nanoparticles were anchored on the HMX surfaces by bidentate chelating bonds in the dopamine solution [33] (Scheme 1).

3.3 Thermal Decomposition Performance of the HMX@PDA@ TiO_2 Composite

Thermal analysis provided a direct measurement of the materials decomposition. Figure 5 shows the DSC curves of HMX and HMX@PDA with different heating rates. The endo-

thermic melting peak for HMX was only partially shown under the 10 Kmin^{-1} and 20 Kmin^{-1} heating rates, indicating that the solid decomposition of HMX would occur before melting under the low heating rates. The decomposition start temperature and peak temperature for HMX were in the range of $252.6\text{--}278.1^\circ\text{C}$ and $273.8\text{--}289.0^\circ\text{C}$, and those for HMX@PDA were in the range of $254.7\text{--}279.4^\circ\text{C}$ and $275.2\text{--}290.1^\circ\text{C}$ under different heating rates. The decom-



Scheme 1. Illustration of the TiO_2 nanoparticles anchored on the HMX surfaces by bidentate chelating bonding.

position exothermic enthalpy was in the range from 1190 Jg^{-1} to 1261 Jg^{-1} for HMX and from 1093 Jg^{-1} to 1273 Jg^{-1} for HMX@PDA, respectively. The HMX crystal structure transition from the β to the δ polymorph was weakened by the polydopamine coating at $181\text{--}188^\circ\text{C}$ [34]. According to the Flynn and Wall method [35], the calculated values of the activation energy were $362.74\text{ kJ mol}^{-1}$ for HMX and 372 kJ mol^{-1} for HMX@PDA in Table 2, respectively, which indicated that the polydopamine coating could not affect the thermal reaction of HMX. Then, the comparative TG-DSC curves at the heating rate of 10 Kmin^{-1} for HMX– TiO_2 were displayed in Figure 6, which demonstrated the typical partial endothermic melting peak and thermal decomposition for HMX. The endothermic effect of -15.45 Jg^{-1} at occurred at 195.9°C , and the exothermic heat of 1279 Jg^{-1} occurred at 283.74°C for HMX– TiO_2 . It showed that the HMX– TiO_2 prepared by electrostatically adsorbing method could not display the catalytic performance for TiO_2 nanoparticles.

However, the bioinspired HMX@PDA@ TiO_2 composites prepared from different dispersion concentrations of TiO_2

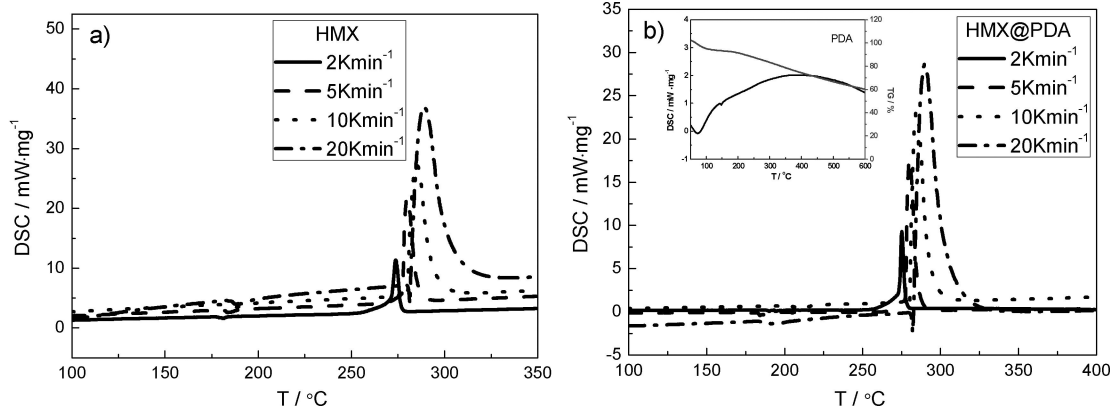
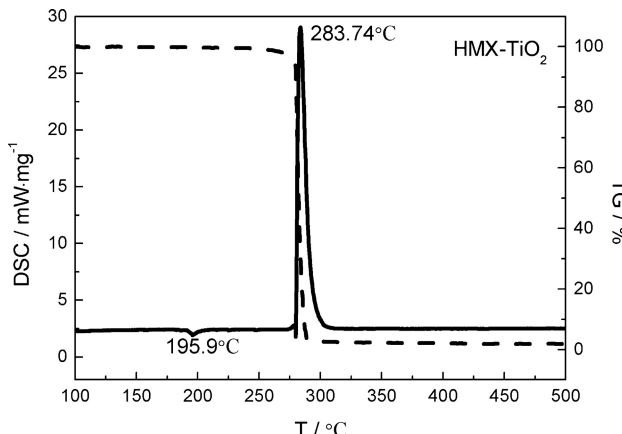


Figure 5. DSC curves of (a) HMX and (b) HMX@PDA with different heating rates (inset image is the pure PDA at a heating rate of $10\text{ }^\circ\text{C min}^{-1}$ under nitrogen atmosphere).

Table 2. Activation energy values for HMX and HMX@PDA.

Sample	Heating rate (Kmin^{-1})	T_t ($^\circ\text{C}$)	Endothermic peak ΔH_t (J g^{-1})	T_s ($^\circ\text{C}$)	T_p ($^\circ\text{C}$)	Exothermic peak ΔH_p (J g^{-1})	E_a (kJ mol^{-1})
HMX	2	181.3	-28.01	252.6	273.8	1321	362.74
	5	183.5	-25.08	263.7	280.1	1190	
	10	187.1	-20.70	270.5	285.1	1199	
	20	188.5	-14.63	278.1	289.0	1261	
HMX@PDA	2	-	-	254.7	275.2	1093	372
	5	-	-	268.4	280.2	1186	
	10	-	-	274.7	285.3	1189	
	20	-	-	279.4	290.1	1273	

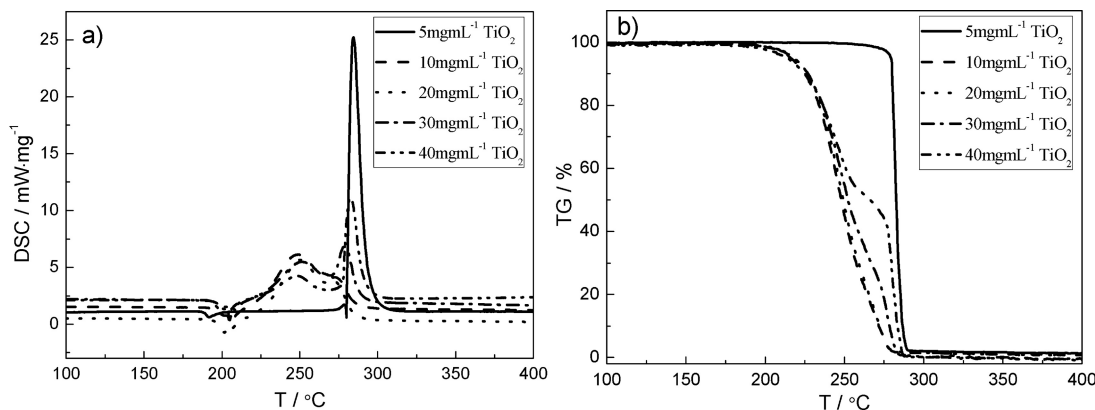
T_t represents the endothermic peak for the crystal structure transition; ΔH_t represents the endothermic enthalpy for the crystal structure transition; T_s represents the starting temperature for the decomposition; T_p represents the exothermic temperature peak for the decomposition; ΔH_p represents the exothermic enthalpy for the decomposition; E_a represents the activation energy for the materials.

Figure 6. TG-DSC curve for HMX-TiO₂.

showed different thermal decomposition processes measured with TG-DSC curves at the heating rate of 10 K min⁻¹ in Figure 7. The decomposition processes for HMX@PDA@TiO₂ were as the same as the processes for HMX, HMX@PDA and HMX-TiO₂ when prepared from the 5 mg mL⁻¹ TiO₂ dispersion, which showed a crystal structure transition endothermic peak at 191.67 °C, and a partial endothermic melting peak, and an exothermic decomposition peak starting at 273.6 °C, owing to fewer TiO₂ nanoparticles covering the HMX surface, as shown in Figure 1 (a,b). When the dis-

persion concentrations of TiO₂ were increased to 10 mg mL⁻¹ and 20 mg mL⁻¹, the decomposition processes for the composites changed. The crystal structure transition processes showed two endothermic peaks at approximately 201 °C and 205 °C, and the endothermic enthalpies increased more than three times. Furthermore, the decomposition processes started at 212.9 °C and 215.5 °C, which were 60 °C lower than that of HMX. Then, the processes showed two exothermic peaks at approximately 249 °C and 272 °C, and the exothermic enthalpies were almost the same with HMX, which indicated that the decomposition processes were divided into two stages, and the peak temperatures decreased approximately 35 °C and 10 °C. When the dispersion concentrations of TiO₂ were increased to 30 mg mL⁻¹ and 40 mg mL⁻¹, the decomposition processes were the same as those of the composites prepared with the 10~20 mg mL⁻¹ TiO₂ dispersions in DSC curves, but different in the exothermic temperature peaks in Table 3, which corresponded to the amount of TiO₂ nanoparticles covering the HMX surfaces. The HMX melting peak was not visible in all DSC curves for the composites prepared with the 10~40 mg mL⁻¹ TiO₂ dispersions, suggesting solid decomposition for the composites. The above TG-DSC curves for the composites indicated that the catalytic effect and the composite pattern of the TiO₂ to HMX affected the decomposition processes of the composites.

In situ FTIR spectra and TG curves under a 10 K min⁻¹ heating rate were measured to detect the gas products of

Figure 7. (a) DSC and (b) TG curves of the HMX@PDA@TiO₂ composites under different dispersion concentrations of TiO₂.Table 3. Exothermic temperature peaks and thermal effects for the HMX@PDA@TiO₂ composites.

Concentrations of TiO ₂ dispersions (mg mL ⁻¹)	T _t (°C) T ₁	T _t T ₂	Endothermic Peak ΔH _t (J g ⁻¹)	T _s (°C) T ₃	T _p (°C) T ₄	Exothermic Peak ΔH _p (J g ⁻¹)	
5	191.67	—	-23.17	273.6	284.45	—	1209
10	201.01	205.22	-78.97	215.5	248.58	272.78	1093
20	201.90	205.40	-69.91	212.9	249.57	271.97	1200
30	201.31	204.93	-82.47	212.1	251.56	278.52	1022
40	198.60	204.94	-66.44	212.2	248.54	282.46	902.5

the composite decomposition at different temperatures in real time. Figure 8 shows the intensities of decomposition gas products with the heating times. The curves suggested that the original HMX decomposed in the range of 26–28 min, while the HMX@PDA@TiO₂ composites were decomposed in the ranges of 19~24 min and 25~27.5 min, which were in keeping with the above TG-DSC curves. According to the specific FTIR spectra of the gas products analysis, HMX decomposed to HCN (713 cm⁻¹), NO₂ (1627 cm⁻¹), HCHO (1743 cm⁻¹), CO (2206 cm⁻¹), N₂O (2237 cm⁻¹) and CO₂ (2310 cm⁻¹) [36,37] in Figure 9. The gas products of the composites were the same as the original HMX, and only the decomposition times were accelerated. The decomposition processes could be first the C–N bond rupture to release HCN, CO₂ and HCHO, followed by the N–N bond rupture to release more NO₂ and N₂O [38]. The FTIR results further confirmed that the bioinspired HMX@PDA@TiO₂ composite could accelerate the decomposition of HMX and not change the decomposition processes.

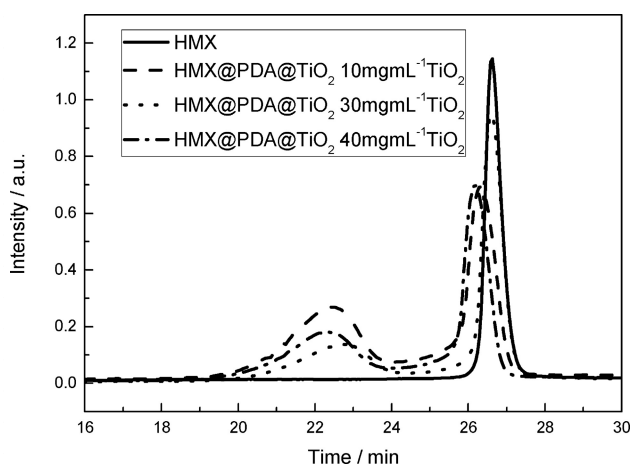


Figure 8. Intensity of gas products for HMX and HMX@PDA@TiO₂ decomposition with heating time under 10 K min⁻¹ heating rate.

Then the combustion performances were compared for the original HMX and HMX@PDA@TiO₂ as showed in Figure 10. Fire-induced ignition had been investigated using 50 mg samples at room ambient, and the fire source was removed once ignited. Energetic material combustion has been experienced with ignited, flame growth, steady burning and flame extinguish [39]. Comparatively, the ignition time and entire combustion duration of HMX@PDA@TiO₂ composites were shorter and longer than those of HMX, but the flame size was smaller. The combustion was corresponded with the above thermal decomposition properties. The composite could be ignited easily for the lower starting decomposition process, and longer burning duration of the composite was closely related to the slower decomposition

process. The bioinspired composition could affect the combustion process of the energetic materials.

4 Conclusion

Inspired by mussel foot adhesion, a HMX@PDA@TiO₂ composite was prepared by a simple solution stirring method to form covalent bonds between TiO₂ nanoparticles and HMX@PDA. The HMX surfaces were homogeneously and closely covered with TiO₂ nanoparticles, and the adhesive nanoparticle mass increased with higher TiO₂ dispersion concentrations. When the concentration of the TiO₂ dispersion was higher than 10 mg mL⁻¹, the obtained composites facilitated the catalytic decomposition of HMX; the starting decomposition temperature was lower, at approximately 60 °C, and the decomposition peak decreased by 35 °C. FTIR results showed that the decomposition products of HMX@PDA@TiO₂ were the same as those with the original HMX. Compared with the decomposition of the original HMX, HMX@PDA and HMX-TiO₂, the composite properties of the bioinspired HMX@PDA@TiO₂ composite had a great effect on the thermal performance. The findings in this study revealed that the interaction properties of the composite greatly influenced the composite performance.

Acknowledgements

This work was supported by the National Natural Science Foundation of China (No. 11772308), the Presidential Foundation of the China Academy of Engineering Physics (YZ2015010), and the Innovation Foundation of the Institute of Chemical Materials (KJCX2014-01).

References

- [1] M. Mukherjee, S. Mukherjee, R. Kumar, R. Shunmugam, Improved thermal and mechanical properties of polynorbornene upon covalent attachment with graphene sheets, *Polymer* **2017**, *123*, 321–333.
- [2] J. Y. Sun, X. Zhao, R. K. Illeperuma Widusha, O. Chaudhuri, K. H. Oh, D. J. Mooney, J. Vlassak, Z. Suo, Highly stretchable and tough hydrogels, *Nature* **2012**, *489*, 133–136.
- [3] S. Park, S. Chang, Catalytic dearomatization of N-heteroarenes with silicon and boron compounds, *Angew. Chem. Int. Ed.* **2017**, *56*, 7720–7738; *Angew. Chem.* **2017**, *129*, 7828–7847.
- [4] X. W. Li, Y. Liu, J. C. Hemminger, R. M. Penner, Catalytically activated palladium@platinum nanowires for accelerated hydrogen gas detection, *ACS Nano* **2015**, *9*, 3215–3225.
- [5] M. Fan, A. Naughton, Mechanisms of thermal decomposition of natural fiber composites, *Composites Part B* **2016**, *88*, 1–10.
- [6] H. F. Cheng, Q. F. Liu, J. Yang, Q. Zhang, R. L. Frost, Thermal behavior and decomposition of kaolinite-potassium acetate intercalation composite, *Thermochim. Acta* **2010**, *503–504*, 16–20.
- [7] W. Choi, A. Tuteja, S. Chhatre, J. M. Mabry, R. E. Cohen, G. H. McKinley, Fabrics with tunable oleophobility, *Adv. Mater.* **2009**, *21*, 2190–2195.

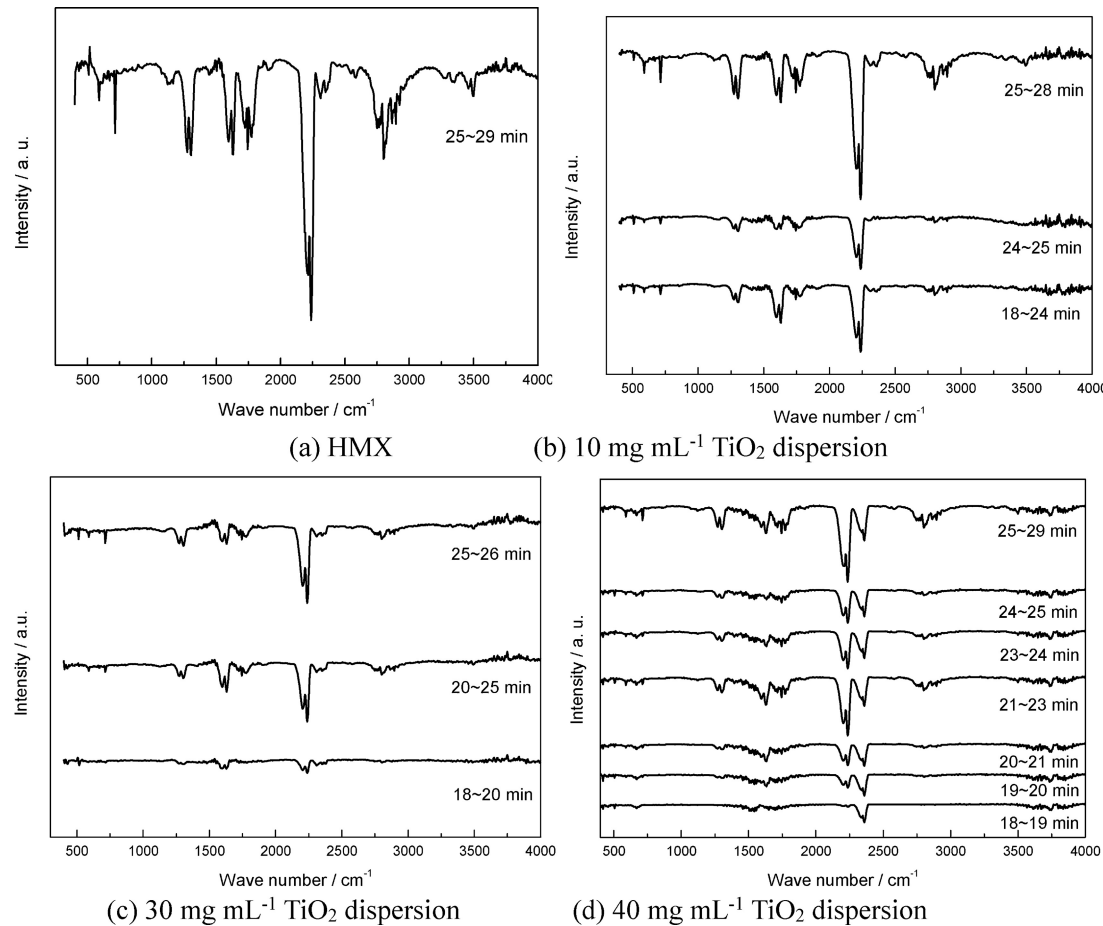


Figure 9. FTIR spectra at different times for HMX and HMX@PDA@ TiO_2 .

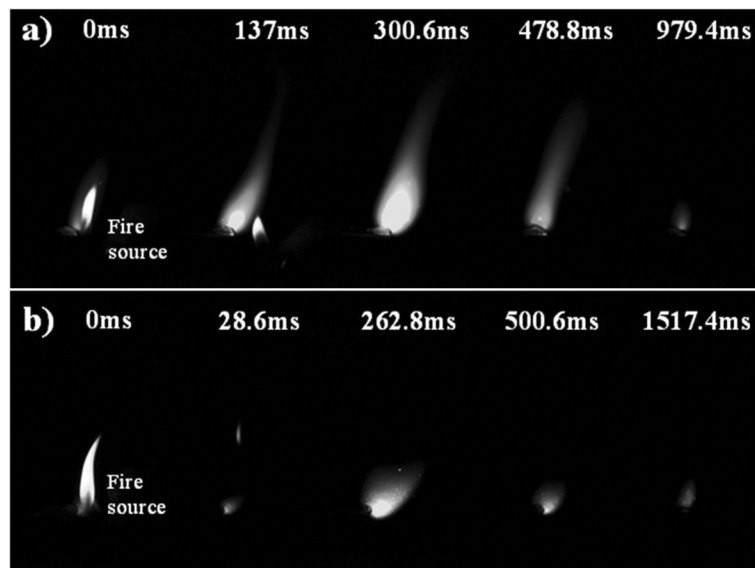


Figure 10. Optical images of combustion for HMX (a) and HMX@PDA@ TiO_2 (b).

- [8] T. Wang, J. Cui, S. Ouyang, W. Cui, S. Wang, A new approach to understand the cassie state of liquids on superamphiphobic materials, *Nanoscale* **2016**, *8*, 3031–3039.
- [9] H. Bellanger, T. Darmanin, E. T. Givenchy, F. Guittard, Chemical and physical pathways for the preparation of superoleophobic surfaces and related wetting theories, *Chem. Rev.* **2014**, *114*, 2694–2716.
- [10] E. Rocha-Rangel, J. A. Rodríguez-García, S. Esparza-Vázquez, B. Cruz-Sánchez, I. Estrada-Guel, R. Martínez-Sánchez, Effect of particle size and titanium content on the fracture toughness of particle-ceramic composites, *Mater. Today: Proceedings* **2016**, *3*, 249–257.
- [11] C. P. Isolan, L. L. Valente, E. A. Münchow, G. R. Basso, A. H. Piamentel, J. K. Schwantz, A. V. Silva, R. R. Moraes, Bond strength of a universal bonding agent and other contemporary dental adhesives applied on enamel, dentin, composite, and porcelain, *Appl. Adh. Sci.* **2014**, *2*, 25.
- [12] G. Yuan, Y. Bai, Z. Jia, D. Hui, K. Lau, Enhancement of interfacial bonding strength of SMA smart composites by using mechanical indented method, *Composites Part B* **2016**, *106*, 99–106.
- [13] X. Xu, Y. Zhang, J. Jiang, H. Wang, X. Zhao, Q. Li, W. Lu, In-situ curing of glass fiber reinforced polymer composites via resistive heating of carbon nanotube films, *Compos. Sci. Technol.* **2017**, *149*, 20–27.
- [14] Q. Zhu, C. Xiao, S. Li, G. Luo, Bioinspired fabrication of insensitive HMX particles with polydopamine coating, *Propellants Explos. Pyrotech.* **2016**, *41*, 1092–1097.
- [15] J. Liu, W. Jiang, F. Li, L. Wang, J. Zeng, Q. Li, Y. Wang, Q. Yang, Effect of drying conditions on the particle size, dispersion state, and mechanical sensitivities of nano HMX, *Propellants Explos. Pyrotech.* **2014**, *39*, 30–39.
- [16] V. P. Sinditsky, On the combustion mechanism of HMX, *Combust. Explos. Shock Waves* **2011**, *47*, 548–552.
- [17] J. R. Deschamps, M. Frisch, D. Parrish, Thermal expansion of HMX, *J. Chem. Crystallogr.* **2011**, *41*, 966–970.
- [18] A. N. Zhigach, I. O. Leipunskii, A. N. Pivkina, N. V. Muravyev, K. A. Monogarov, M. L. Kuskov, E. S. Afanasevskova, N. G. Berezhkina, P. A. Pschenchenkov, A. A. Bragin, Aluminum/HMX nanocomposites: Synthesis, microstructure, and combustion, *Combust. Explos. Shock Waves* **2015**, *51*, 100–106.
- [19] J. Bai, G. Xu, S. Xing, J. Zeng, J. Jiang, Y. Chen, Hydrothermal synthesis and catalytic application of ultrathin rhodium nanosheet nanoassemblies, *ACS Appl. Mater. Interfaces* **2016**, *8*, 33635–33641.
- [20] K. Younes, G. Mehran, Incorporation of TiO₂ coating on a palladium heterogeneous nanocatalyst, A new method to improve reusability of a catalyst, *Catal. Commun.* **2016**, *84*, 16–20.
- [21] R. Shende, S. Subramanian, S. Hasan, S. Apperson, R. Thiruvengadathan, K. Gangopadhyay, S. Gangopadhyay, Nanoenergetic composites of CuO nanorode, nanowires, and Al-nanoparticles, *Propellants Explos. Pyrotech.* **2008**, *33*, 122–130.
- [22] K. Kenji, H. Makoto, Evidence for the anisotropic oxidation of gas-phase Al nanoparticles, *J. Nanopart. Res.* **2015**, *17*, 289–297.
- [23] H. Wang, G. Jian, W. Zhou, J. B. DeLisio, V. T. Lee, M. R. Zachariah, Metal iodate-based energetic composites and their combustion and biocidal performance, *ACS Appl. Mater. Interfaces* **2015**, *7*, 17363–17370.
- [24] C. E. Bunker, M. J. Smith, K. A. S. Fernando, B. A. Harruff, W. K. Lewis, J. R. Gord, E. A. Gulants, D. K. Phelps, Spontaneous hydrogen generation from organic-capped Al nanoparticles and water, *ACS Appl. Mater. Interfaces* **2010**, *2*, 11–14.
- [25] Y. Jing, W. Wei, D. Eric, K. A. Rebekah, N. I. Jacob, J. H. Waite, Mussel protein adhesion depends on interprotein thiol-mediated redox modulation, *Nat. Chem. Biol.* **2011**, *7*, 588–590.
- [26] Q. Zhu, Q. Pan, Mussel-inspired direct immobilization of nanoparticles and application for oil-water separation, *ACS Nano* **2014**, *8*, 1402–1409.
- [27] C. K. Saw, J. M. Zaug, D. L. Farber, B. L. Weeks, C. M. Aracne, Using simultaneous time-resolved SHG and XRD diagnostics to examine phase transitions of HMX and TATB, *AIP Conf. Proc.* **2002**, 856–859.
- [28] Y. Dong, X. Fei, Z. Liu, Y. Zhou, L. Cao, Synthesis and photocatalytic redox properties of anatase TiO₂ single crystals, *Appl. Surf. Sci.* **2017**, *394*, 386–393.
- [29] G. L. Wang, J. J. Xu, H. Y. Chen, Dopamine sensitized nanoporous TiO₂ film on electrodes: Photoelectrochemical sensing of NADH under visible irradiation, *Biosens. Bioelectron.* **2009**, *24*, 2494–2498.
- [30] B. Zhu, S. Edmondson, Polydopamine-melanin initiators for surface-initiated ATRP, *Polymer* **2011**, *52*, 2141–2149.
- [31] J. Zhao, W. Xing, Y. Li, K. Lu, Solvothermal synthesis and visible light absorption of anatase TiO₂, *Mater. Lett.* **2015**, *145*, 332–335.
- [32] X. Li, J. Li, Y. Li, K. Xia, Surface modification and characterization of 8-hydroxyquinoline aluminum/nano-TiO₂, *J. Lumin.* **2016**, *171*, 131–137.
- [33] Q. Ye, F. Zhou, W. Liu, Bioinspired catecholic chemistry for surface modification, *Chem. Soc. Rev.* **2011**, *40*, 4244–4258.
- [34] B. L. Korsunskii, S. M. Aldoshin, S. A. Vozchikova, N. I. Golovina, N. V. Chukanov, G. V. Shilov, A New Crystalline HMX polymorph: ε-HMX, *Russ. J. Phys. Chem. B* **2010**, 934.
- [35] C. Popescu, Integral method to analyze the kinetics of heterogeneous reactions under non-isothermal conditions A variant on the Ozawa-Flynn-Wall method, *Thermochim. Acta* **1996**, *285*, 309–313.
- [36] H. Jiang, L. P. Zhu, L. J. Zhu, B. K. Zhu, Y. Y. Xu, Surface characteristics of a self-polymerized dopamine coating deposited on hydrophobic polymer films, *Langmuir* **2011**, *27*, 14180–14187.
- [37] X. Y. Liu, X. C. Wang, Y. G. Huang, M. X. Zheng, L. Wang, Y. Jiang, Y. W. Luo, Study on thermal decomposition of HMX energetic materials by in-situ FTIR spectroscopy, *Spectrosc. Spectr. Anal.* **2006**, *26*, 251.
- [38] A. K. Burnham, R. K. Weese, Thermal decomposition kinetics of HMX, *36th Int. Annual Conference of ICT and 32nd International Pyrotechnics Seminar*, Karlsruhe, Germany, June 28–July 1, **2005**, 25–1.
- [39] K. V. Meredith, M. L. Gross, M. W. Beckstead, Laser-induced ignition modeling of HMX, *Combust. Flame* **2015**, *162*, 506–515.

Manuscript received: September 10, 2018

Revised manuscript received: November 13, 2018

Version of record online: January 29, 2019